Cavitation Threshold Evaluation of Porcine Cerebrospinal Fluid using a Polymeric Split Hopkinson Pressure Bar-Confinement Chamber Apparatus

M.C. Bustamante[a], D.S. Cronin[b]

[a]mcbustam@uwaterloo.ca; [b]duane.cronin@uwaterloo.ca

[a,b]Department of Mechanical Engineering, University of Waterloo, 200 University Ave. W., Waterloo, ON, N2L3G1

Declarations of interest: none

Abstract

Studies investigating mild Traumatic Brain Injury (mTBI) in the military population using experimental head surrogates and Finite Element (FE) head models have demonstrated the existence of transient negative pressures occurring within the head at the *contrecoup* location to the blast wave impingement. It has been hypothesized that this negative pressure may cause cavitation of cerebrospinal fluid (CSF) and possibly lead to brain tissue damage from cavitation bubble collapse. The cavitation pressure threshold of human CSF is presently unknown, although existing FE studies in the literature have assumed a value of -100 kPa. In the present study, the cavitation threshold of degassed porcine CSF at body temperature (37°C) was measured using a unique modified Polymeric Split Hopkinson Pressure Bar apparatus, and compared to thresholds of distilled water at various conditions. The loading pulse generated in the apparatus was comparable to experimentally measured pressures resulting from blast exposure, and those predicted by an FE model. The occurrence of cavitation was identified using high-speed imaging and the corresponding pressures were determined using a computational model of the apparatus that was previously developed and validated. The probability of cavitation was calculated (ISO/TS 18506) from forty-one experimental tests on porcine CSF, representing an upper bound for *in vivo* CSF. The 50% probability of cavitation for CSF (-0.467 MPa ±7%) was lower than that of distilled water (-1.37 MPa ±16%) under the same conditions. The lesser threshold of CSF could be related to the constituents such as blood cells and proteins. The results of this study can be used to inform FE head models subjected to blast exposure and improve prediction of the potential for CSF cavitation and response of brain tissue.

Keywords: Cavitation; Porcine Cerebrospinal Fluid; Polymeric Split Hopkinson Pressure Bar; Mild Traumatic Brain Injury; Negative Intracranial Pressure

1 Introduction and Background

Traumatic brain injury associated with blast exposure is common in military conflicts due to the use of Improvised Explosive Devices (IEDs) such as roadside bombs. A broad overview of the casualties during Operation Enduring Freedom in Afghanistan and Operation Iraqi Freedom in Iraq reveals that about 80% of all casualties resulted from blast exposure, and about 40% of service member fatalities resulted from IEDs [1, 2]. The United States Department of Defence categorizes mild Traumatic Brain Injury (mTBI) as a loss of consciousness for up to 30 minutes and an alteration of consciousness or mental state for up to 24 hours [3]. The Defence and Veterans Brain Injury Center reported that, as of 2017, 85% of all worldwide TBI cases diagnosed in U.S. forces were categorized as mild [4].

There is currently no consensus regarding mechanisms that cause mTBI associated with blast exposure. Current theories include damage from the shearing of soft-tissue [5–8], distortion of brain tissue cellular structures and cells [6, 9–15], and intracranial fluid cavitation [6, 16–20]. There have been a number of blast exposure studies in the literature that have reported negative pressures occurring at the *contrecoup* location of head blast exposure, demonstrating the possibility of cavitation [17, 20–29]. For example, Singh et al. (2014) reported negative pressures at the *contrecoup* ranging between -0.211 and -0.769 MPa that were predicted using validated FE head models exposed to blasts at 3 to 4 m standoff distances [20]. Wave theory suggests that the negative pressure is the result of the incident compressive pressure pulse propagating through the head, and reflecting at the *contrecoup* in tension due to the greater impedance of the head relative to the surrounding air [21]. Some studies have suggested that the negative pressure is greatly exacerbated by flexure of the skull [17, 23, 26]. However, Panzer et al. (2012) reported no evidence of localized skull flexure using a plane-strain head model and predicted large localized positive pressures in the brain having an assumed CSF cavitation threshold of -0.10 MPa, modeled as a tensile pressure cut-off threshold. A histological study reported scarring in postmortem brain tissues from military service members exposed to blast at similar locations to those reported by Panzer [30].

Some studies have explored the effects of cavitation damage on brain tissue by inducing cavitation collapse on a seed bubble purposefully introduced into the surrounding fluid. Damage such as tears and disruptions along the cell layers of tissue from the cavitation collapse of a seeded bubble have been reported on rat brain tissue immersed in artificial CSF [31]. Similarly, an FE study modeled preexisting seed bubbles within a brain tissue matrix and reported the potential for axonal fiber damage resulting from cavitation and collapse of the seed bubble [32]. The cavitation pressure threshold of human CSF is not possible to measure *in vivo*, has not been measured in PMHS, nor has it been measured *in vitro*. Therefore, it is currently not possible to assess the likelihood of cavitation from head blast exposure. In the present study, a validated method and test apparatus were used to measure the cavitation threshold of degassed porcine CSF at body temperature (37°C).

1.1 Background on Cavitation

Cavitation is the nucleation, expansion, and collapse of bubbles within a fluid that occurs when the pressure in a fluid of constant temperature drops below a critical pressure, known as the cavitation pressure threshold. Cavitation can result from either homogeneous or heterogeneous nucleation. Homogeneous nucleation occurs when a vapor phase appears from the separation of fluid molecules and reaches a stable critical radius permitting growth. On the other hand, heterogeneous nucleation occurs when a cavity nucleates from existing weaknesses in the system such as suspended particles, dissolved gases, and entrapped air [33, 34]. Heterogeneous nucleation occurs at lesser cavitation pressure thresholds due to such weaknesses acting as nucleation sites, whereas homogeneous nucleation occurs at the tensile strength of the fluid. It is very difficult to observe cavitation from homogeneous nucleation because, even in laboratory conditions, it is difficult to remove all the weaknesses from a system. Therefore, the more common occurrence of cavitation is the result of heterogeneous nucleation, and the reported thresholds have a large variability due to the differences in the experimental methods such as loading rate, surface roughness, and differences in fluid conditions such as temperature and purity. Due to these many factors, the cavitation threshold is often expressed as the probability of cavitation, and therefore large sets of data points are required to determine a representative value of the cavitation pressure threshold [33, 35–37]**.** Negative pressures are often transient and the subsequent rise to positive pressure can lead to the collapse of the cavities known as micro-jetting, which produces high localized positive pressure that is known to damage surrounding solid materials [16, 38–43].

1.2 Previous Measurement of Cavitation Pressure using Transient Loading

There are many dynamic methods of generating cavitation existing in the literature including, the tube-arrest [44–46], the bullet-piston [47–51], and the fluid-Hopkinson bar [52] methods. A recent study by the authors reviewed these methods discussing their advantages and limitations, and developed an apparatus for evaluating localized fluid cavitation using a modified Polymeric Split Hopkinson Pressure Bar coupled with a fluid confinement chamber [37]. The apparatus was called the Closed-Chamber Modified Cavitation Hopkinson Bar (C3HB) and was developed to overcome the limitation of the existing methods relating to the loading pulse magnitude and shape, fluid volume requirement, and boundary conditions compared to blast exposure.

The C3HB apparatus consisted of a steel sphere striker, a PolyMethylMethAcrylate (PMMA) incident bar, and a PMMA confinement chamber (**Fig 1**). The combination of the steel sphere striker and PMMA incident bar consistently produced a compressive pressure pulse comparable to that measured at the *coup* location of frontal head blast exposure [37]. This approach was advantageous since achieving the incident pulse required no major modifications to the Hopkinson bar apparatus, whereas both the tube-arrest and bullet-piston methods would require replacements involving a different length tube and piston rod, respectively.

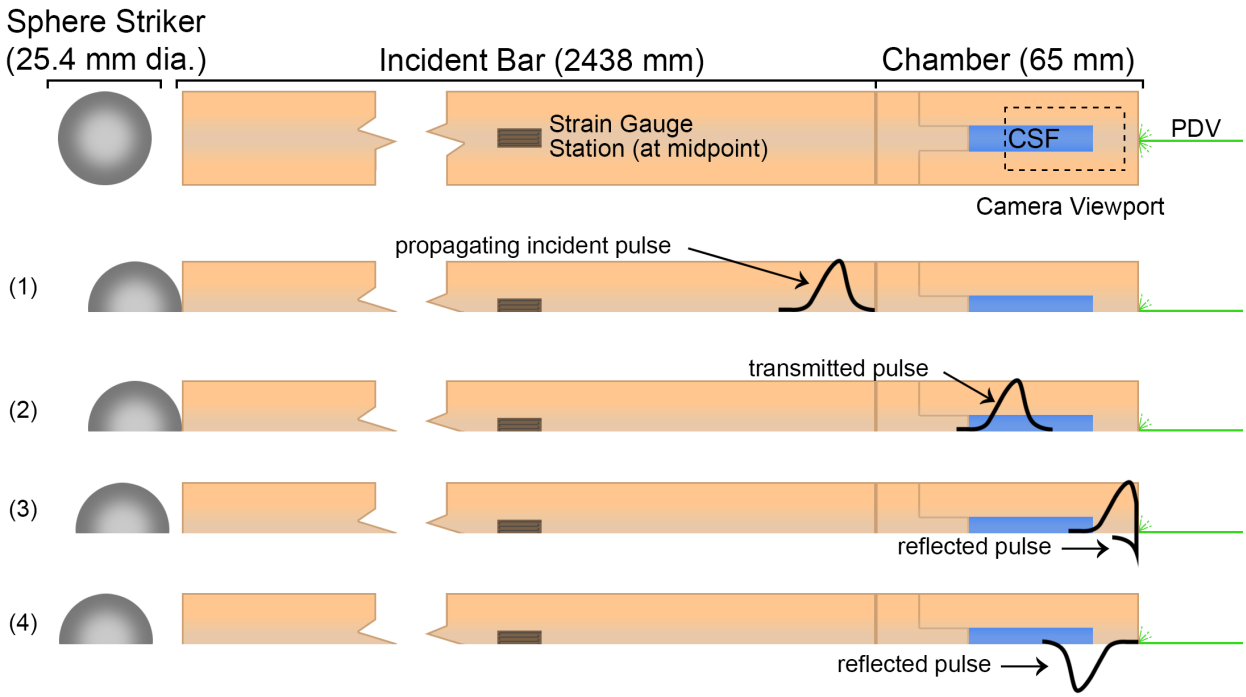

Fig 1 Diagram of the C3HB apparatus indicating the locations of the instrumentation; and the simplified propagation of the incident pulse resulting in a negative reflected pulse. Note that the amplitudes and periods of the pulses are simplified and not representative of those measured

Although changes to the Hopkinson bar section of the C3HB were straightforward, design of the fluid confinement chamber was far more involved. The confinement chamber was designed for low volume testing (~1 mL of fluid) and to provide a greater acoustic impedance boundary condition, which was similar to the *contrecoup* location of the head in blast exposure [37]. The low volume requirement was advantageous when testing difficult to obtain biological fluids such as CSF. The C3HB produced localized cavitation in the fluid adjacent to the greater impedance boundary of the chamber, which was desired because of its similarity to the boundary conditions of CSF adjacent to the skull. Additionally, the high impedance boundary was important for the hypothesized mechanism that the negative pressure observed in head blast exposure results from a compressive pulse reflecting in tension.

Operation of the C3HB consisted of accelerating the sphere striker towards the incident bar and generating an incident pulse (compressive) that propagated down the bar and into the confinement chamber filled with CSF (**Fig 1 (1)**). Figure 1 illustrates the generation of the pulse reflection hypothesized as the primary mechanism that produces negative fluid pressure. The pulse entering the chamber is denoted as the transmitted pulse (compression) (**Fig 1 (2)**) and the pulse resulting from the reflection at the free surface of the chamber (chamber-end) is denoted as the reflected pulse (tensile) (**Fig 1 (4)**).

Wave theory shows that energies and senses of transmitted and reflected pulses from an incident pulse propagating through an interface are governed by the acoustic impedance difference of the two mediums creating the interface [53]. The transmitted pulse is always the same sense as the

incident pulse, whereas the sense of the reflected pulse is the same when the incident pulse enters a greater impedance medium and the opposite when the incident pulse enters a lesser impedance medium. Further detail of the pulse propagation within the chamber was as follows. Upon passing through four interfaces with changing impedances, all the incident pulse energies were separated into their corresponding transmitted and reflected pulses (**Fig 2**). Note that the transmitted pulses become incident pulses when entering a new interface. The incident pulse generated by the striker impact propagated through the cap and transmitted into the CSF (**Fig 2 (1)**). This transmitted pulse then propagated to the back-wall interface transmitting some energy into the chamber back-wall while reflecting some energy back towards the cap (**Fig 2 (2)**). The pulse in the back-wall reflected in tension at the atmosphere interface and, due to the far lesser impedance of air relative to PMMA, was a total reflection of the incident pulse (**Fig 2 (3)**). Lastly, this tensile pulse reflection was transmitted into the CSF generating negative pressure (**Fig 2 (4)**). The apparatus generated negative pressure in a volume ~ 2 mm from the back-wall, denoted as the cavitation zone. The duration of the negative pressure was approximately 0.15 ms, which was comparable to those reported to have generated cavitation [31].

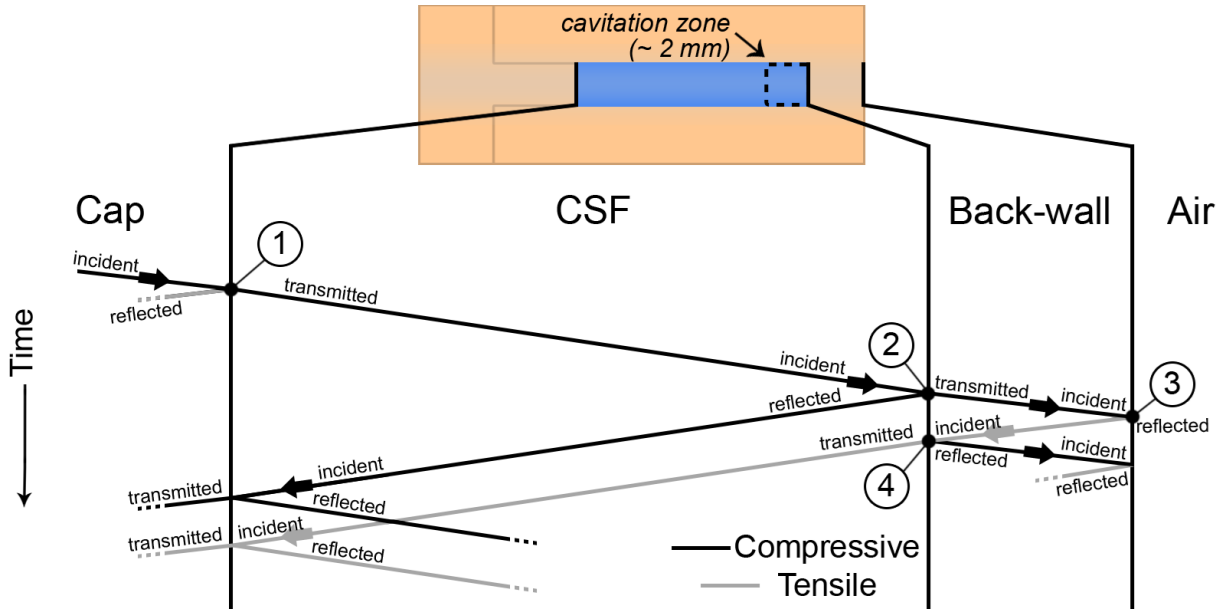

Fig 2 Wave diagram of the propagating pulses within the chamber. Dotted lines indicate pulses that continue, but are not shown for clarity. Incident pulse separations are shown at four different times: (1) chamber cap to CSF, (2) CSF to chamber back-wall, (3) back-wall to atmospheric air, and (4) back-wall to CSF

The pulse propagation in the PMMA bars of the FE model was validated using 24 experimental tests with varying striker velocities and types [54]. Agreement of the simulated bar strains with those measured in the experimental tests was checked using cross-correlation [55, 56], which yielded ratings ranging between 0.97 and 0.997, where a rating of 1.0 is a perfect correlation. The same validation process was performed on the simulated chamber strain against 27 experimental tests of varying striker velocities that yielded a cross-correlation rating of 0.921 [37]. A common evaluation of model fit for biofidelity of anthropomorphic test dummies defined in ISO/TR 9790 [57] identifies scores ranging between 0.86 and 1.0 as Excellent, between 0.65 and 0.86 as Good, between 0.44 and 0.65 as Fair, between 0.26 and 0.44 as Marginal, and between 0 and 0.26 as

Unacceptable. Thus, the cross-correlation score computed for the PMMA bars in the FE model validation cases using the system defined in the standard indicated Excellent agreement with experimental measurements.

During the development of the C3HB, issues related to the direct measurement of fluid pressure were recognized using both piezoelectric probe-style (PCB Model 113B21, PCB Piezotronics) and piezoresistive catheter-style (SPR-524 Mikro-Tip Catheter Transducers, Millar, Inc.) pressure transducers. Both transducers demonstrated an inability to accurately measure negative (tensile) fluid pressure and geometric discontinuities introduced by the presence of the transducers created nucleation sites, lower the cavitation threshold, and producing erroneous results [37]. Therefore, the chamber and fluid was included in the FE model of the apparatus and was developed to predict the fluid pressure based on direct measurements. These measurements were strain taken at the incident bar by the strain gauge station; surface velocity at the chamber-end taken by the PDV (**Fig 1**); and strain at the midpoint of the chamber taken by an additional strain gauge station, thereby mitigating the need for a physical transducer within the fluid [37, 54]. The negative fluid pressure was obtained from the fluid elements adjacent to the chamber back-wall within the cavitation zone (**Fig 2**). It should be noted that the initiation and collapse of cavitation bubbles were not implemented into the FE model, and therefore, the model only predicted the maximum negative fluid pressure expected if the fluid remained continuous [37].

Initial fluid cavitation tests were performed with the C3HB apparatus by filling the chamber with distilled water at 21°C and including a thin film of a wetting agent on the inner-surface of the chamber (side-walls) to reduce entrapped air [37]. Seventy-seven distilled water cavitation experimental tests were re-created using the FE model and a cavitation threshold of -3.32 MPa ±3% was measured (distilled water with a wetting agent). In a preliminary study [58], untreated distilled water at 21°C, degassed distilled water at 37°C, and distilled water with a wetting agent at 37°C, were tested to investigate the effects of their treatment on the cavitation pressure threshold. Untreated distilled water at 21°C yielded a cavitation pressure threshold of -0.53 MPa ±25%, degassed distilled water at 37°C yielded -1.37 MPa ±16%, and distilled water at 37°C with a wetting agent yielded -3.195 MPa ±5%. [37, 58]. This preliminary study demonstrated that the conditions and preparation of the fluid had a large effect on the cavitation threshold.

Overall, evidence exists for the potential of cavitation due to negative intracranial pressure resulting from blast exposure, and could potentially lead to brain tissue damage in the vicinity of the cavitation event. The cavitation pressure threshold of human CSF is currently unknown, and the determination of a threshold is critical to assessing the probability for cavitation in a given blast scenario. The present study builds upon the past journal article detailing the development of the C3HB apparatus and the preliminary study investigating fluid treatments on distilled water. In the present study, the cavitation pressure threshold of degassed porcine CSF at body temperature (37°C) was measured using the C3HB apparatus.

2 Methods

The C3HB apparatus [37] was used in the present study (**Fig 1**). Strain gauges (CEA-13-250UW-120, Micro-Measurements) mounted at the midpoint of the incident bar measured the propagating strain pulses and the data was amplified (2210B Signal Conditioning Amplifier, Vishay) and recorded (BNC-2110, National Instruments) at 2 MHz. Additionally, a Photon Doppler Velocimeter (PDV) (1550 nm wavelength, Ohio Manufacturing Institute) probe was directed at the chamber-end surface to measure its surface velocity at a sample rate of 10 MHz. A high-speed camera (FASTCAM SA5 Model 1300K-M1, Photron, 50,000 fps with 512x272 resolution) was oriented perpendicular to the chamber to capture the occurrence of cavitation (**Fig 1**) [37].

The negative fluid pressure at the *contrecoup* location was calculated using a first-order approximation (Equation 1) as a verification of the FE model predictions [37]. The approximation made the assumptions that: (1) the pulse propagation between the chamber and CSF was one-dimensional; (2) the back-wall chamber surface had an equal velocity as the chamber-end, and (3) the pulses transmitted from the CSF to the chamber cap did not reflect back into the CSF within the time period considered. Equation 1 used: the CSF density (ρ_{CSF}); the acoustic wave speeds of the acrylic ($C_{o_{acrylic}}$) and CSF ($C_{o_{CSF}}$); the surface velocity of the chamber-end that was measured by the PDV ($v(t)$); and the calculated percentage of energy transmitted from the acrylic to the CSF (η). The velocity terms $v(t_{-1})$ and $v(t_{-2})$ correspond to velocity values that are 1 and 2 timesteps before v(t), respectively. It was assumed that the CSF at 37°C behaved similarly to water at 37°C and a bulk modulus of 2.282 GPa and density of 1.00 g/cm^3 was used to represent the fluid [59–61]. The acrylic acoustic wave speed (2193 m/s) was calculated with measured propagating distances and arrival times of the strain pulses in the apparatus. The CSF acoustic wave speed (1511 m/s) was estimated from bulk modulus and density based on water at 37°C.

$$P_{backwall}(t) = \left(-\rho_{CSF} * C_{o_{acrylic}} * \left(v(t) - v(t_{-1})\right)\right) + \left(-\rho_{CSF} * C_{o_{CSF}} * \eta * \left(v(t_{-1}) - v(t_{-2})\right)\right) \quad \text{Equation 1}$$

Equation 1 was derived from a small cylindrical volume of CSF that was bounded by the acrylic back wall and additional CSF, respectively. The change in pressure of the small volume was calculated using the change in surface velocities of the faces as the pressure wave propagated from the acrylic to the CSF boundary (assumption 1). The first term of the equation represented the pressure from the change in velocity of the acrylic boundary and the second term represented the pressure from the change in velocity of the CSF boundary; therefore, their summation equaled the change in pressure of the volume. This approximation was compared to the numerical predictions of the fluid negative pressure and yielded a good agreement.

Porcine CSF was used because it was more readily available than human CSF, and swine models for studying TBI have been established in the literature [62–66], although porcine CSF has a larger number of white blood cells and proteins relative to human CSF [67]. Porcine CSF was supplied by the Defence Research and Development Canada, Suffield Research Centre, and was obtained from castrated male York-Landrace cross swine (~20 kg) for research conducted according to the "Guide to the Care and Use of Experimental Animals" and the "Ethics of animal Experimentation"

published by the Canadian Council on Animal Care. The animals were anesthetized (5% isoflurane in 100% oxygen) and CSF was drawn and immediately frozen and shipped on dry ice to the laboratory facilities. The CSF was stored frozen up to the time it was tested. The CSF was defrosted at room temperature for 24 hours and then placed into a water bath at 37°C for at least 1 hour before use. Prior to undertaking a test, the empty chamber was thoroughly cleaned using distilled water and a light solution of soap to remove grease. The chamber was then rinsed with distilled water and thoroughly dried. The chamber was slowly and carefully filled with the porcine CSF at 37°C using a syringe, ensuring that there was no entrapped air visible. The CSF-filled chamber (specimen) was then degassed. A degassed treatment was considered because a wetting agent treatment would have resulted in chemical contamination of the CSF constituents, and a previous study on distilled water demonstrated that a degassing treatment yielded a cavitation threshold variability 156% lesser than without treatment [58]. Initial tests on untreated CSF produced high variability and led to cavitation, even with the weakest impact possible with the apparatus. Since a non-cavitating event was not possible, a threshold could not be established; however, many of these tests yielded cavitation at tensile pressures below one atmosphere (101.3 kPa).

Degassing was performed by placing the chamber specimen into a glass container connected directly to a vacuum pump using a hose (**Fig 3**). A vacuum gauge connected to the hose was used to measure the gauge pressure within the system and an inlet with a gate valve that allowed atmospheric air into the system was connected to the hose for controlling and maintaining the negative pressure. For the given setup, a pressure of -0.093 MPa was determined to be the optimal gauge pressure to remove entrapped air within the CSF without causing boiling. This optimal pressure was determined by slowly increasing the negative pressure in the container, by way of closing the gate valve, just before aggressive boiling occurred. A degassing period of 20 minutes at -0.093 MPa was used because it was determined through visual inspection that at approximately 20 minutes the CSF was still and gas was no longer escaping.

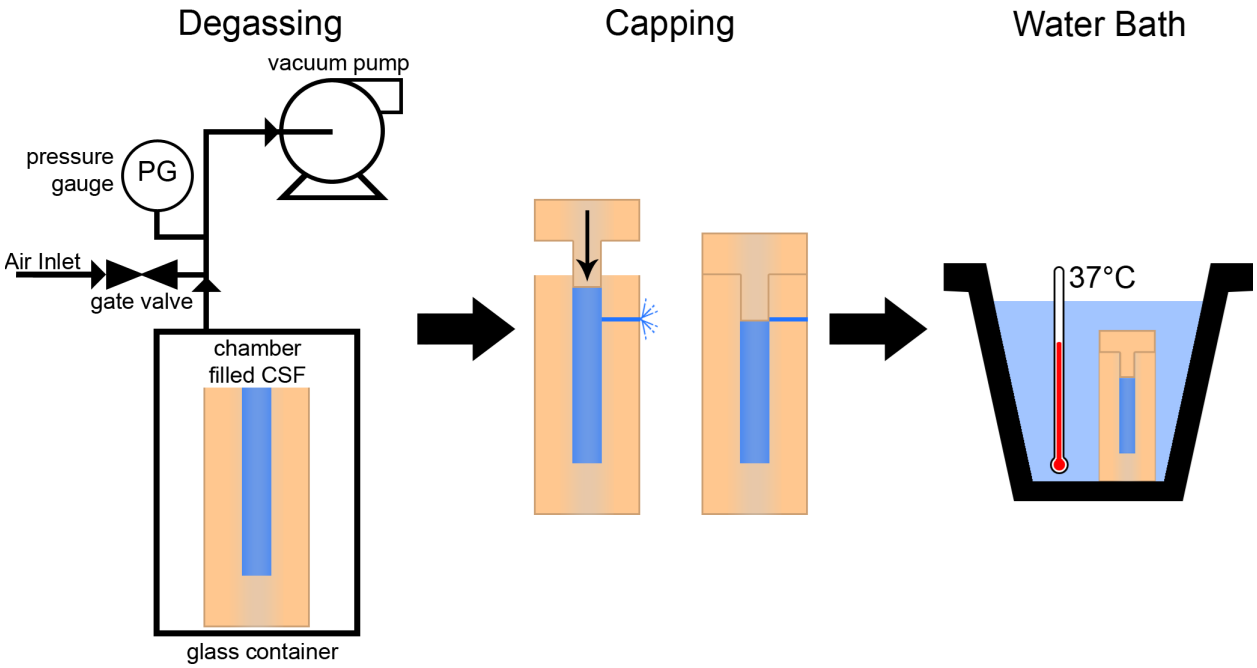

Fig 3 Illustration of the degassing, capping, and water bath procedures that were undertaken to prepare a single chamber sample filled with CSF

Once degassing was completed, the pressure in the glass container was slowly brought to atmospheric pressure by way of opening the gate valve and then the specimen was quickly removed and capped. A vent channel at the side of the chamber expelled CSF during capping and ensured the chamber was completely full of fluid and upon full insertion of the cap, the stem would block the channel creating an enclosed system; this design feature was described in greater detail in [37]. It should be noted that there was an opportunity for air to diffuse into the CSF during the time of removing the specimen from the glass container and capping; therefore, the amount of time spent degassing and capping was made consistent throughout the entire study. Once capped, the specimen was submerged into another water bath at 37°C for at least 30 minutes. Expulsion of the CSF from the chamber as a result of reheating was not observed suggesting that the degassing process did not reduce the CSF temperature considerably from its initial 37°C temperature prior to degassing.

After 30 minutes of being submerged in the 37°C water bath, the chamber specimen was quickly removed and dried. The chamber was placed at the end of the incident bar with Petroleum Jelly used as a coupling agent to ensure full contact and to relieve frictional forces [10, 68]. The time between removing the specimen from the water bath to firing the striker was consistently below 2 minutes and an infrared thermometer was used immediately before each test to verify the specimen temperature of 37°C.

Preparation of the C3HB apparatus and instrumentation was performed during the final water bath. Recordings of the incident bar strain gauge and PDV measurements were triggered by the propagating incident pulse. Sufficient pre-triggering samples were also recorded to ensure the entire event was captured. The high-speed imaging of the chamber was triggered when movement was detected through the change in brightness level of a specified area in the viewport. Syncing of

the high-speed imaging with the recorded strain gauge and PDV measurements were performed in post-processing by tracking (Tracker v4.9.8, Open Source Physics) the chamber-end surface movement and syncing it with the PDV measurement.

The same test protocol detailed in [37] was performed. After each test, cavitation was noted from the captured high-speed imaging. The test was considered to have exhibited cavitation when at least one bubble nucleated within the cavitation zone, where negative pressure was expected, before bulk movement of the chamber (**Fig 2**). If cavitation was observed, the CSF was discarded, and a new specimen was prepared, otherwise, the specimen was placed back into the 37°C water bath for at least 5 minutes to ensure the sample was at 37°C prior to performing another test. For all tests performed, the negative fluid pressure at the back-wall of the chamber was predicted using the FE model based on the incident pulse measured by the incident bar strain gauge station as the input. Additionally, the predicted chamber-end velocity was verified against the PDV measurement and the predicted fluid pressure was verified against the first-order approximation discussed earlier. Similar to the study [37], each predicted pressure was paired with a binary data point corresponding to cavitation or no cavitation observed. A sigmoid probability curve was calculated using the paired data points with the process outlined in ISO/TS 18506 to obtain the 50% probability of cavitation [69]. This 50% probability of cavitation was then considered as the measured cavitation pressure threshold for the set of the cavitation tests.

3 Results & Discussion

In a typical experimental test where cavitation did not occur, the high-speed video exhibited no signs of bubble formation or fluid movement. In a typical experimental test where cavitation did occur, the high-speed video exhibited cavitation as 1 to 3 individual bubbles with maximum diameters no greater than ~1 mm, or as bubble clusters (**Fig 4**). Tests, where bubbles nucleated outside the cavitation zone but not inside the cavitation zone, were considered to be non-cavitating events because weaknesses in the fluid may have promoted nucleation since it did not occur at the peak negative pressure within the zone. Inspection of the chamber specimens post-test also exhibited evidence of cavitation in the form of stable bubble clusters floating in the CSF, whereas the non-cavitating tests did not.

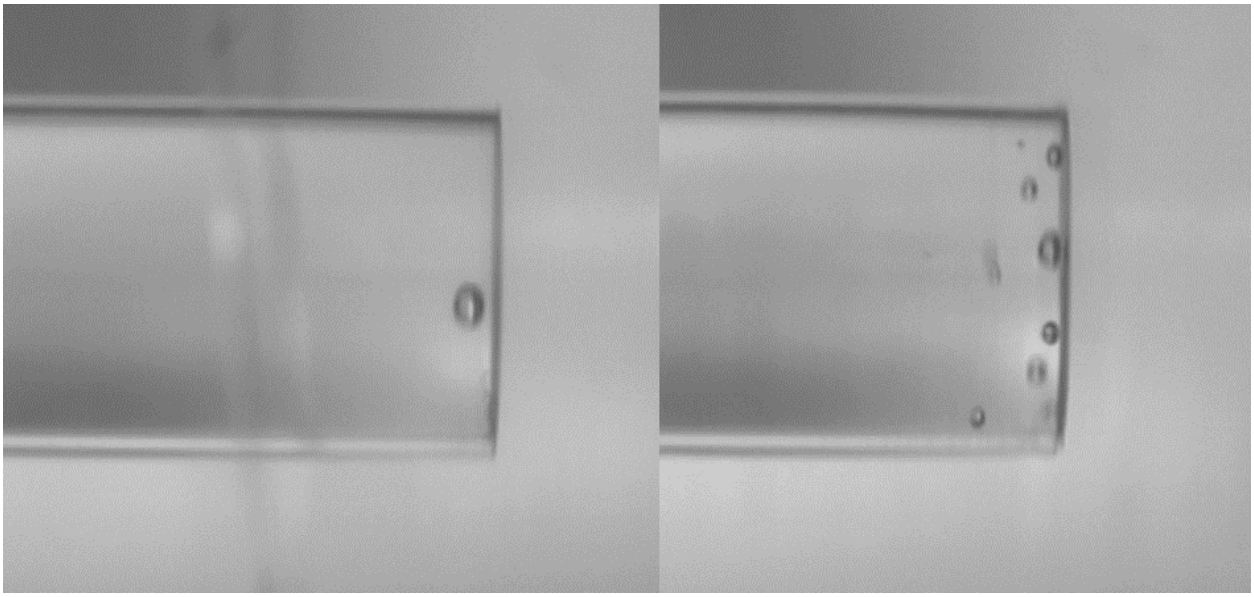

Fig 4 High-speed image of a test producing an individual cavitation bubble (left) and a test producing a cavitation bubble cluster (right)

Using the full supply of the available CSF, forty-one tests were performed on degassed porcine CSF at 37º C yielding a cavitation pressure threshold of -0.467 MPa ±7%, which corresponded to the negative pressure at which there was 50% probability of cavitation occurring (**Fig 5**). Since CSF contains dissolved gases, it should be expected that the threshold of CSF *in vivo* would be lesser than the upper-bound measured in the present study. For example, the cavitation threshold of distilled water reported in [58] decreased from -1.37 MPa ±16% to -0.53 MPa ±25% for degassed to an untreated (as-received) condition. If a similar decreasing trend of ~60% was applicable to the degassed CSF threshold measured, porcine CSF in an untreated condition would yield a predicted threshold of approximately -0.180 MPa, which is on the order of the speculated -0.100 MPa threshold noted in the literature. However, it is quite possible that the untreated cavitation limit could be even lower due to dissolved gases and solids present in the CSF that can act as nucleation sites. It should be further noted that the values quoted are 50% probabilities, and that cavitation can occur at lower pressures.

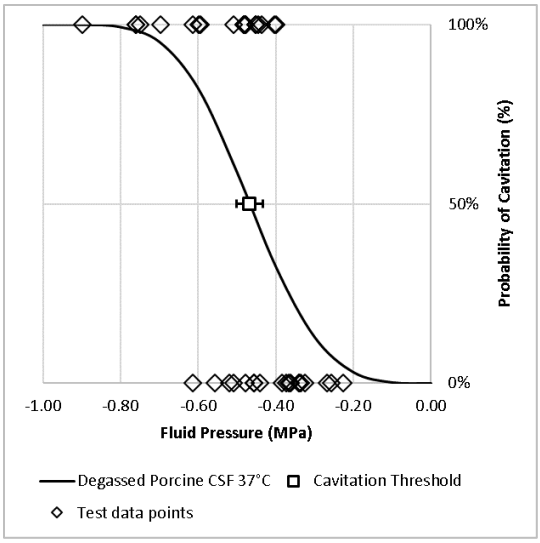

Fig 5 The measured cavitation threshold and probability curve from 41 individual experimental tests of porcine CSF at body temperature (Error bars show one standard deviation)

Furthermore, a discrepancy was observed between the measured threshold for porcine CSF and that reported for distilled water [58] with both at 37°C and degassed. CSF is comprised of 99% water, can carry dissolved oxygen and carbon dioxide [70–72], but with a composition similar to blood plasma [67, 73–76]. Such a similarity to water led to the speculated cavitation threshold of -0.100 MPa often cited within the literature [18, 26, 77]. Thus, it was expected that CSF (-0.467 MPa ±7%) and distilled water (-1.37 MPa ±16%) at the same conditions would yield similar cavitation pressure thresholds. However, more tests resulted in cavitation at negative pressures between approximately -0.5 and -1.0 MPa in the CSF than in the distilled water at the same conditions (**Fig 6**), suggesting that solids such as cells and proteins within CSF may reduce the cavitation threshold. Therefore, the decrease in the threshold between degassed and untreated porcine CSF may be greater than the ~60% decrease observed between the degassed and untreated distilled water.

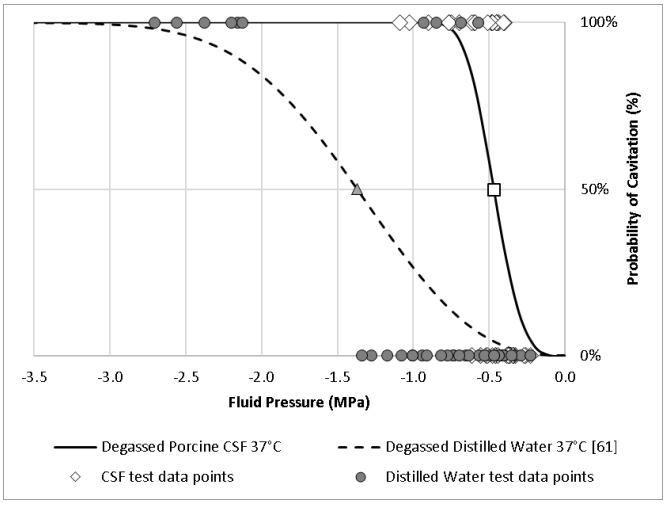

Fig 6 Cavitation thresholds, probability curves, and experimental data points of porcine CSF and distilled water [58], both degassed and at body temperature

For an ideal injury risk curve, there would be a step-wise transition from 0% to 100% probability at the measured threshold. The faster transition from 0% to 100% probability of cavitation exhibited by the CSF curve relative to the distilled water curve indicates that there was less scatter in the CSF datapoints, and in other words there was less overlap of the 0% and 100% datapoints for CSF than for distilled water (**Fig 6**). This was further emphasized by the 7% (0.034 MPa) standard deviation of the CSF threshold versus the 16% (0.216 MPa) of the distilled water. However, further investigation is required to adequately provide an explanation for the considerable difference in scattering between the measured thresholds of CSF and distilled water at the same fluid conditions. The CSF yielded a threshold most comparable to that of untreated distilled water at 21°C (-0.53 MPa ±25%), albeit the CSF threshold having a lesser standard deviation (**Fig 7**). Perhaps suspended solids within the CSF reduced the threshold in a similar amount, as the dissolved gases within the distilled water, but the concentration of the solids in the CSF was lesser than that of the dissolved gases in the distilled water; thus, more investigation is required.

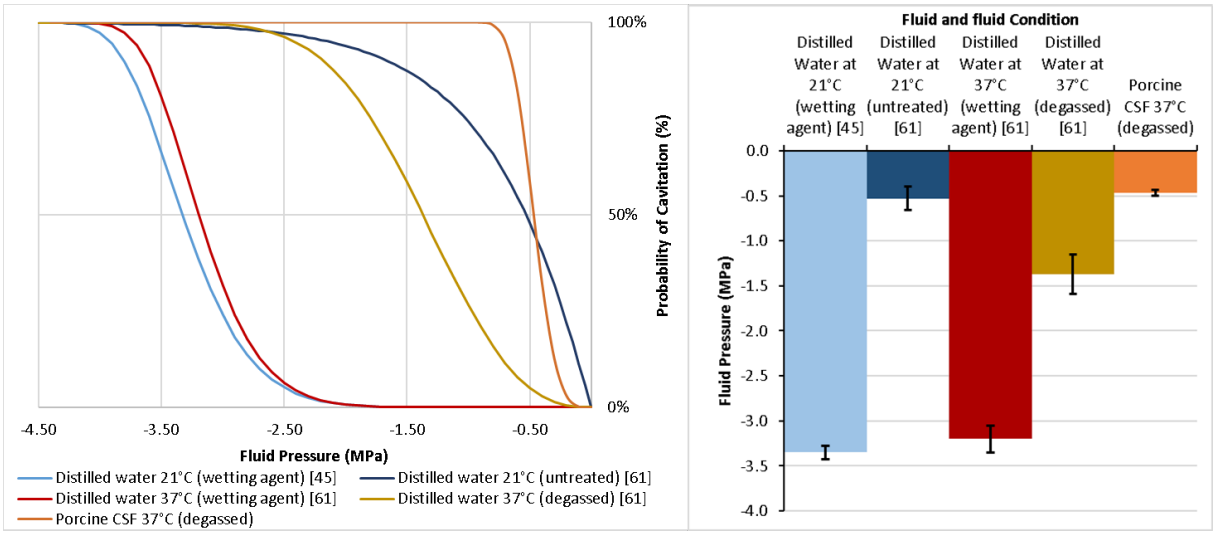

Fig 7 Cavitation threshold probability curves and bar chart of distilled water at various treatment and temperature conditions and porcine CSF in the present study. Error bars show one standard deviation

To determine the potential for CSF cavitation in blast exposure, the probability of cavitation from the sigmoid curve calculated in the present study was compared to the survivability from a set of Bowen curves for a body perpendicular to the blast winds in an open-field [78]. Reported information from existing experimental and computational studies in the literature was used to calculate the probabilities of cavitation and survivability for varying blast conditions. The probabilities of CSF cavitation were calculated using the reported peak *contre-coup* negative pressures and the survivability were calculated using the reported overpressures and durations from the existing literature (**Table 1**). This comparison used frontal blast exposure cases from the experimental shock tube tests on cadaver heads by Bir (2011) [22], the computational FE free-field blast exposure tests on planar head models by Singh et al. (2014) [20], and the computation FE free-field blast exposure tests on a three-dimensional head model by Zhang et al. (2013) [29].

The three overpressures (71, 76, and 104 kPa) reported by Bir for frontal blast exposure fell below the threshold value for lung injury on the Bowen curves and yielded ~0% probability of cavitation. The 170 kPa overpressure case reported by Singh also fell below the threshold value for lung injury on the Bowen curves and yielded 4% probability of cavitation. The 326 kPa overpressure reported by. Singh yielded <1% probability of fatality using the Bowen curves and 35% probability of CSF cavitation. Lastly, the four overpressures (270, 350, 460, and 660 kPa) reported by Zhang yielded 14%, 37%, 32%, and 53% probability of cavitation; while the probability of fatality was <1% for all four overpressures when assessed using the Bowen curves [29]. However, the calculated probabilities of cavitation may be conservative, since they were calculated using the data from degassed CSF while non-degassed CSF may represent a lower bound for *in vivo* conditions. When a probability curve for non-degassed CSF was extrapolated from the degassed CSF, based on the previous tests on distilled water, the probabilities of cavitation increased in all cases. The three overpressures reported by Bir slightly increase but remained ~0%, the two overpressures reported by Singh increase from 4% to 6%, and 35% to 58%; and the four overpressure reported by Zhang increase from 53% to 89%, 32% to 54%, 37% to 62%, and 14% to 24%. The probabilities of cavitation for all overpressures considered were equal to or far greater than that the probability of fatality determined using the Bowen curves, thus demonstrating that intracranial cavitation is a potential source of injury in unprotected blast exposure, and could occur in blast events when the probabilities of survivability are high.

Table 1 Summary of probability analysis for intracranial cavitation and lung damage from Bowen curves

Study	Duration (ms)	Overpressure (kPa)	Peak *contre-coup* negative ICP (kPa)	Probability of Cavitation using degassed CSF (%)	Estimated Probability of Cavitation using non-degassed CSF (%)	Bowen curves - Body perpendicular to blast winds (Probability of fatality %)	Bowen curves - Body perpendicular to blast winds (fatality %)
Bir (2011)	~7.5	71	-30	0%	0%	Below lung injury threshold line	Below damage threshold line
	~7.5	76	-38	0%	0%	Below lung injury threshold line	Below damage threshold line
	~7.5	104	-30	0%	0%	Below lung injury threshold line	Below damage threshold line
Singh et al. (2014)	~3	170	-211	4%	6%	Below lung injury threshold line	Below damage threshold line
	~3	326	-410	35%	58%	<1%	<1%
Zhang et al. (2013)	1	660	-480	53%	89%	<1%	<1%
	1.5	460	-400	32%	54%	<1%	<1%
	2	350	-420	37%	62%	<1%	<1%
	3	270	-310	14%	24%	<1%	<1%

The findings of the current study introduce an opportunity for future work in testing untreated porcine CSF and investigating the effects of the solid constituents on the threshold. Such a study in measuring the cavitation threshold of untreated porcine CSF would provide further insight into the probability of cavitation occurring *in vivo* and may provide a realistic lower-bound threshold. A limitation of the current study that should be noted was that no composition analysis was performed on the CSF and the variability between the animals may have affected the results.

4 Conclusions

A series of cavitation tests were undertaken on degassed porcine CSF to generate a cavitation probability curve at body temperature using the C3HB apparatus. Since degassed porcine CSF was used, an upper-bound cavitation pressure threshold of -0.467 MPa ±7% was measured, corresponding to the negative pressure with a 50% probability of generating cavitation in CSF as a result of loading comparable to that observed in head blast exposure. The measured threshold for porcine CSF was less than a previously reported threshold for distilled water (-1.37 MPa ±16%) under the same temperature and degassed condition, albeit CSF being comprised of 99% water. It was hypothesized that the difference in thresholds was attributed to the solid constituents of CSF that do not exist in distilled water. Further investigation is required for re-creating CSF conditions comparable to *in vivo*; however, this study provides empirical data as additional insight to the speculated threshold used in head models exposed to blast and can be applied to future studies to provide knowledge representing the upper-bound response to CSF cavitation.

Acknowledgments

The authors would like to acknowledge the Defence Research and Development Canada, Suffield Research Centre for supplying materials, the Natural Sciences and Engineering Research Council of Canada for financial support, and Compute Canada and Sharcnet for providing the necessary computing resources.

5 References

1. White M (2003) iCasualties : Iraq Coalition Casualty Count. http://www.icasualties.org. Accessed 1 Jun 2018

2. Owens BD, Kragh JF, Wenke JC, et al (2008) Combat wounds in operation Iraqi Freedom and operation Enduring Freedom. J Trauma 64:295–9. https://doi.org/10.1097/TA.0b013e318163b875

3. The Management of Concussion-mild Traumatic Brain Injury Working Group (2016) VA/DoD Clinical Practice Guideline for the Management of Concussion-mild Traumatic Brain Injury. U.S. Department of Veterans Affairs, Washington DC

4. Defence and Veterans Brain Injury Center (2016) DoD Worldwide Numbers for TBI. http://dvbic.dcoe.mil/dod-worldwide-numbers-tbi. Accessed 3 May 2018

5. Alley MD, Schimizze BR, Son SF (2011) Experimental modeling of explosive blast-related traumatic brain injuries. Neuroimage 54:S45–S54. https://doi.org/10.1016/j.neuroimage.2010.05.030

6. Sarntinoranont M, Lee SJ, Hong Y, et al (2012) High-Strain-Rate Brain Injury Model Using Submerged Acute Rat Brain Tissue Slices. J Neurotrauma 29:418–429. https://doi.org/10.1089/neu.2011.1772

7. Nie X, Sanborn B, Weerasooriya T, Chen W (2013) High-rate bulk and shear responses of bovine brain tissue. Int J Impact Eng 53:56–61. https://doi.org/10.1016/j.ijimpeng.2012.07.012

8. Sosa M a G, De Gasperi R, Paulino AJ, et al (2013) Blast overpressure induces shear-related injuries in the brain of rats exposed to a mild traumatic brain injury. Acta Neuropathol Commun 1:51. https://doi.org/10.1186/2051-5960-1-51

9. Ling G, Bandak F, Armonda R, et al (2009) Explosive blast neurotrauma. J Neurotrauma 26:815–825. https://doi.org/10.1089/neu.2007.0484

10. Bo C, Balzer J, Brown K a., et al (2011) Development of a chamber to investigate high-intensity compression waves upon live cell cultures. Eur Phys J Appl Phys 55:31201. https://doi.org/10.1051/epjap/2011110052

11. Risling M, Plantman S, Angeria M, et al (2011) Mechanisms of blast induced brain injuries, experimental studies in rats. Neuroimage 54:S89-97. https://doi.org/10.1016/j.neuroimage.2010.05.031

12. Bolander R, Mathie B, Bir C, et al (2011) Skull flexure as a contributing factor in the mechanism of injury in the rat when exposed to a shock wave. Ann Biomed Eng 39:2550–2559. https://doi.org/10.1007/s10439-011-0343-0

13. Ryu J, Horkayne-Szakaly I, Xu L, et al (2014) The problem of axonal injury in the brains of veterans with histories of blast exposure. Acta Neuropathol Commun 2:153. https://doi.org/10.1186/s40478-014-0153-3

14. Heldt SA, Elberger AJ, Deng Y, et al (2014) A novel closed-head model of mild traumatic

brain injury caused by primary overpressure blast to the cranium produces sustained emotional deficits in mice. Front Neurol 5 JAN:1–14. https://doi.org/10.3389/fneur.2014.00002

15. Kamnaksh A, Budde MD, Kovesdi E, et al (2014) Diffusion tensor imaging reveals acute subcortical changes after mild blast-induced traumatic brain injury. Sci Rep 4:4809. https://doi.org/10.1038/srep04809

16. Lee CS, Frizzell LA (1988) Exposure levels for ultrasonic cavitation in the mouse neonate. Ultrasound Med Biol 14:735–742. https://doi.org/10.1016/0301-5629(88)90029-4

17. Goeller J, Wardlaw A, Treichler D, et al (2012) Investigation of Cavitation as a Possible Damage Mechanism in Blast-Induced Traumatic Brain Injury. J Neurotrauma 29:1970–1981. https://doi.org/10.1089/neu.2011.2224

18. Panzer MB, Myers BS, Capehart BP, Bass CR (2012) Development of a finite element model for blast brain injury and the effects of CSF cavitation. Ann Biomed Eng 40:1530–1544. https://doi.org/10.1007/s10439-012-0519-2

19. Hong Y, Sarntinoranont M, Subhash G, et al (2015) Localized Tissue Surrogate Deformation due to Controlled Single Bubble Cavitation. Exp Mech 97–109. https://doi.org/10.1007/s11340-015-0024-2

20. Singh D, Cronin DS, Haladuick TN (2014) Head and brain response to blast using sagittal and transverse finite element models. Int j numer method biomed eng 30:470–489. https://doi.org/10.1002/cnm.2612

21. Zhu F, Mao H, Dal Cengio Leonardi A, et al (2010) Development of an FE model of the rat head subjected to air shock loading. Stapp Car Crash J 54:211–225. https://doi.org/2010-22-0011 [pii]

22. Bir C (2011) Measuring Blast-Related Intracranial Pressure Within the Human Head. Detroit, MI

23. Ganpule S, Alai A, Plougonven E, Chandra N (2013) Mechanics of blast loading on the head models in the study of traumatic brain injury using experimental and computational approaches. Biomech Model Mechanobiol 12:511–531. https://doi.org/10.1007/s10237-012-0421-8

24. Grujicic M, Arakere G, He T (2010) Material-modeling and structural-mechanics aspects of the traumatic brain injury problem. Multidiscip Model Mater Struct 6:335–363. https://doi.org/10.1108/15736101011080097

25. Hua Y, Kumar Akula P, Gu L, et al (2014) Experimental and Numerical Investigation of the Mechanism of Blast Wave Transmission Through a Surrogate Head. J Comput Nonlinear Dyn 9:031010. https://doi.org/10.1115/1.4026156

26. Moss WC, King MJ, Blackman EG (2009) Skull flexure from blast waves: A mechanism for brain injury with implications for helmet design. Phys Rev Lett 103:4–7. https://doi.org/10.1103/PhysRevLett.103.108702

27. Panzer MB, Bass CR, Myers BS (2010) Numerical Study on the Role of Helmet Protection

in Blast Brain Injury. In: Personal Armor Systems Symposium. Quebec City, Canada, p 11

28. Sayed T El, Mota A, Fraternali F, Ortiz M (2008) Biomechanics of traumatic brain injury. Comput Methods Appl Mech Eng 197:4692–4701. https://doi.org/10.1016/j.cma.2008.06.006

29. Zhang L, Makwana R, Sharma S (2013) Brain response to primary blast wave using validated finite element models of human head and advanced combat helmet. Front Neurol 4 AUG:88. https://doi.org/10.3389/fneur.2013.00088

30. Shively SB, Horkayne-Szakaly I, Jones R V., et al (2016) Characterisation of interface astroglial scarring in the human brain after blast exposure: a post-mortem case series. Lancet Neurol 15:944–953. https://doi.org/10.1016/S1474-4422(16)30057-6

31. Canchi S, Kelly K, Hong Y, et al (2017) Controlled single bubble cavitation collapse results in jet-induced injury in brain tissue. J Mech Behav Biomed Mater 74:261–273. https://doi.org/10.1016/j.jmbbm.2017.06.018

32. Haniff S, Taylor PA (2017) In silico investigation of blast-induced intracranial fluid cavitation as it potentially leads to traumatic brain injury. Shock Waves 27:929–945. https://doi.org/10.1007/s00193-017-0765-1

33. Brennen CE (2013) Cavitation and Bubble Dynamics. Cambridge University Press, Cambridge

34. Kenner VH, Wieczorek DC (1980) The Response of Blood to Transient Tensile Loading. J Biomech Eng 102:151–154

35. Caupin F, Herbert E (2006) Cavitation in water: a review. Comptes Rendus Phys 7:1000–1017. https://doi.org/10.1016/j.crhy.2006.10.015

36. Williams PR, Williams RL (2004) Cavitation and the tensile strength of liquids under dynamic stressing. Mol Phys 102:2091–2102. https://doi.org/10.1080/00268970412331292786

37. Bustamante MC, Singh D, Cronin DS (2017) Polymeric Hopkinson Bar-Confinement Chamber Apparatus to Evaluate Fluid Cavitation. Exp Mech 1–20. https://doi.org/10.1007/s11340-017-0323-x

38. Chahine KKG (2014) Advanced Experimental and Numerical Techniques for Cavitation Erosion Prediction. 106:3–35, 71–95. https://doi.org/10.1007/978-94-017-8539-6

39. Zhu Y, Zou J, Zhao WL, et al (2016) A study on surface topography in cavitation erosion tests of AlSi10Mg. Tribol Int 102:419–428. https://doi.org/10.1016/j.triboint.2016.06.007

40. Fry FJ, Sanghvi NT, Foster RS, et al (1995) Ultrasound and microbubbles: Their generation, detection and potential utilization in tissue and organ therapy-Experimental. Ultrasound Med Biol 21:1227–1237. https://doi.org/10.1016/0301-5629(96)89519-6

41. Ginsberg HJ, Drake JM, Cobbold RSC (2001) Unblocking cerebrospinal fluid shunts using low frequency ultrasonic cavitation. In: 2001 IEEE Ultrasonics Symposium. Proceedings. An International Symposium (Cat. No.01CH37263). IEEE, pp 1381–1384

42. Zhang C, Huang P, Zhang Y, et al (2014) Anti-tumor efficacy of ultrasonic cavitation is potentiated by concurrent delivery of anti-angiogenic drug in colon cancer. Cancer Lett 347:105–113. https://doi.org/10.1016/j.canlet.2014.01.022

43. Tsaklis P (2010) Presentation of Acoustic Waves Propagation and Their Effects Through Human Body Tissues. Hum Mov 11:91–95. https://doi.org/10.2478/v10038-009-0025-z

44. Chesterman WD (1952) The Dynamics of Small Transient Cavities. Proc Phys Soc 65:846–858. https://doi.org/10.1088/0370-1301/65/11/302

45. Overton GDN, Williams PR, Trevena DH (1984) The influence of cavitation history and entrained gas on liquid tensile strength. J Phys D Appl Phys 17:979–987. https://doi.org/10.1088/0022-3727/17/5/012

46. Williams PR, Williams PM, Brown SWJ, Temperley HN V. (1999) On the tensile strength of water under pulsed dynamic stressing. Proc R Soc A Math Phys Eng Sci 455:3311–3323. https://doi.org/10.1098/rspa.1999.0452

47. Bull TH (1956) The tensile strengths of viscous liquids under dynamic loading. Br J Appl Phys 7:416–418. https://doi.org/10.1088/0508-3443/7/11/308

48. Couzens DCF, Trevena DH (1969) Critical Tension in a Liquid under Dynamic Conditions of Stressing. Nature 222:473–474. https://doi.org/10.1038/222473a0

49. Sedgewick SA, Trevena DH (1978) Breaking tensions of dilute polyacrylamide solutions. J Phys D Appl Phys 11:2517–2526. https://doi.org/10.1088/0022-3727/11/18/010

50. Overton GDN, Treverna DH (1982) Some factors which influence the observed dynamic breaking tensions of a liquid. J Phys D Appl Phys 15:3–6. https://doi.org/10.1088/0022-3727/15/2/001

51. Strand OT, Berzins L V, Goosman DR, et al (2004) Velocitimetry using heterodyne techniques. SPIE Proc 5580:593–599. https://doi.org/10.1117/12.567579

52. Kenner VH (1980) The fluid Hopkinson bar. Exp Mech 20:226–232. https://doi.org/10.1007/BF02327705

53. Kolsky H (1949) An Investigation of the Mechanical Properties of Materials at very High Rates of Loading. Proc Phys Soc Sect B 62:676–700. https://doi.org/10.1088/0370-1301/62/11/302

54. Bustamante M, Cronin DS, Singh D (2018) Experimental Testing and Computational Analysis of Viscoelastic Wave Propagation in Polymeric Split Hopkinson Pressure Bar. In: Kimberley J, Lamberson L, Mates S (eds). Dynamic Behavior of Materials, Volume 1. Conference Proceedings of the Society for Experimental Mechanics Series, pp 67–72

55. Thunert C (2012) CORA Release 3.6 User ’s Manual. Ingolstadt, Germany

56. Gehre C, Gades H, Wernicke P (2009) Objective rating of signals using test and simulation responses. In: Enhanced Safety Vehicle (ESV). National Highway Traffic Safety Administration, Stuttgart, Germany

57. (1999) ISO/TR 9790: Road Vehicles – Anthropomorphic side impact dummy – lateral

impact response requirements to assess the biofidelity of the dummy. Geneva

58. Bustamante MC, Cronin DS (2019) Assessment of Fluid Cavitation Threshold Using a Polymeric Split Hopkinson Bar-Confinement Chamber Apparatus. In: Conference Proceedings of the Society for Experimental Mechanics Series. pp 95–99

59. Ganpule S, Cao G, Gu L, Chandra N (2009) The effect of shock wave on a human head. In: ASME 2009 International Mechanical Engineering Congress and Exposition (IMECE2009). Florida, USA, p 8

60. Williams PR, Williams PM, Brown SW (1998) Cavitation phenomena in water involving the reflection of ultrasound pulses from a free surface, or from flexible membranes. Phys Med Biol 43:3101–3111. https://doi.org/10.1088/0031-9155/43/10/028

61. Finnemore EJ, Franzini JB (2001) Properties of Fluids. In: Fluid Mechanics with Engineering Applications, 10th ed. McGraw-Hill Higher Education, Boston, p 816

62. Ahmed F, Gyorgy A, Kamnaksh A, et al (2012) Time-dependent changes of protein biomarker levels in the cerebrospinal fluid after blast traumatic brain injury. Electrophoresis 33:3705–3711. https://doi.org/10.1002/elps.201200299

63. Bauman R a, Ling G, Tong L, et al (2009) An introductory characterization of a combat-casualty-care relevant swine model of closed head injury resulting from exposure to explosive blast. J Neurotrauma 26:841–860. https://doi.org/10.1089/neu.2009-0898

64. Gyorgy A, Ling G, Wingo D, et al (2011) Time-Dependent Changes in Serum Biomarker Levels after Blast Traumatic Brain Injury. J Neurotrauma 28:1121–1126. https://doi.org/10.1089/neu.2010.1561

65. De Lanerolle NC, Bandak F, Kang D, et al (2011) Characteristics of an explosive blast-induced brain injury in an experimental model. J Neuropathol Exp Neurol 70:1046–1057. https://doi.org/10.1097/NEN.0b013e318235bef2

66. Manley GT, Rosenthal G, Lam M, et al (2006) Controlled Cortical Impact in Swine: Pathophysiology and Biomechanics. J Neurotrauma 23:128–139. https://doi.org/10.1089/neu.2006.23.128

67. Altman PL (1961) Blood and other body fluids : analysis and compilation. Federation of American Societies for Experimental Biology, Washington, DC

68. Zhang J, Yoganandan N, Pintar FA, et al (2011) Effects of tissue preservation temperature on high strain-rate material properties of brain. J Biomech 44:391–396. https://doi.org/10.1016/j.jbiomech.2010.10.024

69. ISO/TS (2014) ISO/TS 18506 Procedure to construct injury risk curves for the evaluation of road user protection in crash tests. International Organization for Standardization (ISO), Geneva, Switzerland

70. Skinhøj E (1965) Cisternal Fluid Oxygen Tension in Man. Acta Neurol Scand 41:313–318. https://doi.org/10.1111/j.1600-0404.1965.tb01893.x

71. Venkatesh B, Boots RJ (1997) Carbon dioxide and oxygen partial pressure measurements

in the cerebrospinal fluid in a conventional blood gas analyzer: Analysis of bias and precision. J Neurol Sci 147:5–8. https://doi.org/10.1016/S0022-510X(96)05304-X

72. Bradley RD, Semple SJG (1962) A comparison of certain acid-base characteristics of arterial blood, jugular venous blood and cerebrospinal fluid in man, and the effect on them of some acute and chronic acid-base disturbances. J Physiol 160:381–391. https://doi.org/10.1113/jphysiol.1962.sp006853

73. Conn PM (2008) Neuroscience in Medicine, Third. Humana Press, Totowa, NJ

74. Marieb ENE, Hoehn K (2010) Human Anatomy & Physiology, 8th ed. Pearson Education, San Francisco, CA

75. Kandel ER, Kandel ER, Schwartz JH, et al (2000) Principles of Neural Science, 5th ed. McGraw-Hill Medical, New York

76. Jurado R, Walker HK (1990) Cerebrospinal Fluid, 3rd ed. Butterworth Publishers, Boston

77. Lubock P, Goldsmith W (1980) Experimental cavitation studies in a model head-neck system. J Biomech 13:1041–1052. https://doi.org/10.1016/0021-9290(80)90048-2

78. Bowen IG, Fletcher ER, Richmond DR (1968) Estimate of man's tolerance to the direct effects of air blast. Albuquerque, NM